water

MDPI

Article

Metal Leaching from Canal-Top Photovoltaic Modules Under Outdoor Static Water Immersion: Experimental Evidence and Water-Quality Implications for a Drinking-Water Transfer Canal

An Zhou [1], Lekang Ma [2], Yuling Huang [2,*], Huihuang Luo [2], Xiaodong Song [1], Leiming Meng [1], Zhenghao Liu [1] and Qianjin Yang [2]

[1] China South-to-North Water Diversion Renewables Investment Corporation Limited, Beijing 100073, China; zhouan@csnwd.com.cn (A.Z.); songxiaodong@csnwd.com.cn (X.S.); mengleiming@csnwd.com.cn (L.M.); liu-zhenghao@csnwd.com.cn (Z.L.)

[2] China Institute of Water Resources and Hydropower Research, Beijing 100038, China; malekang@ctgu.edu.cn (L.M.); luohh@iwhr.com (H.L.); qianjin.yang@st.gxu.edu.cn (Q.Y.)

* Correspondence: hylcos90@gmail.com

Abstract

Installing solar corridors (photovoltaic, PV) over drinking-water transfer canals can combine renewable power with land and water savings, but direct module-water contact raises questions about metal release and water-quality safety. Two-season outdoor static-immersion experiments were conducted with commercial crystalline-silicon modules (LONGi P-type, TOPCon and IBC; CHINT TOPCon), intact and damaged. In autumn (8 d), only As and Ni were detectable (0.22–0.35 and 0.53–2.60 μg/L); As stabilized within 12–24 h, whereas Ni rose gradually, and Pb, Cd and phenol were only sporadically detected near detection limits. In spring (66 d), Cu, Fe, Mn, Zn, As and Ni were released at μg/L levels (maxima 105, 48, 6.6, 5.9, 1.0 and 2.4 μg/L, respectively), with Cd, Cr(VI) and Hg undetectable. Cu dominated, exceeding the GB 3838-2002 Class I limit (10 μg/L) but remaining well below Class II and drinking-water limits (1.0 mg/L). Fe, Mn and Zn peaked within 6 d, whereas Cu showed a unique corrosion-driven secondary-release phase at 8–17 d, stabilizing only after 24 d. Damage severity did not monotonically control release in the single pools tested; the intact-module pool showed the highest Cu, Mn and Ni, pointing to corrosion of exposed Cu-bearing components. Scaling measured fluxes to a 350 m^3/s canal discharge (1 km corridor) gives steady-state increments of ~10^{-4} μg/L for the campaign-average release rate and ~4×10^{-3} μg/L for the maximum observed interval-rate scenario, both far below regulatory limits, supporting a low water-quality risk for the measured analytes under the tested conditions, as measured in the context of this limited study.

Keywords: photovoltaic module; leaching; heavy metals; water quality; canal-top photovoltaic

Check for updates

Academic Editors: Katarzyna Pietrucha-Urbanik and Janusz Rak

Received: 29 September 2026
Revised: 27 October 2026
Accepted: 29 October 2026
Published: 1 November 2026

Copyright: © 2026 by the authors. Licensee MDPI, Basel, Switzerland. This article is an open access article distributed under the terms and conditions of the Creative Commons Attribution (CC BY) license.

1. Introduction

Photovoltaic (PV) capacity has expanded rapidly over the past decade, and the land footprint of ground-mounted plants has intensified competition for land resources. Deploying PV over water surfaces—floating photovoltaics (FPV) on reservoirs, lakes and ponds—and canal-top PV over irrigation or transfer canals has emerged as a way to relieve this constraint while generating additional co-benefits [1–4]. Covering canals with PV panels has been shown to reduce evaporative water losses, suppress aquatic weed growth and cool the panels, improving energy yield [5]. Operationally, the first canal-top plants

were built over irrigation canals in Gujarat, India, where a 1 MW system spans a 750 m canal section and a 10 MW system spans 3.5 km [6], and long-term monitoring has validated the performance and degradation behavior of such systems [7]. In the United States, the Project Nexus pilot over Californian canals is testing these co-benefits at scale, following the regional simulations of McKuin et al. [5].

China is now considering a far more consequential application: building PV corridors over a long-distance open canal water transfer project (LDWTP), which delivers drinking water to more than 58 million people along its path [8]. The canal's water quality has been maintained at an "excellent" level with an average water-quality index of 90.39 over 2016–2019 [8,9]. The concentrations of 18 heavy metals along the main canal between 2018 and 2020 were found to be below the GB 3838-2002 Class I limits [10,11]. Because the canal conveys drinking-water source water, any infrastructure placed above or in contact with the water must be demonstrated not to compromise this quality.

The environmental literature on over-water PV has so far focused on physical and biological effects, including shading, reduced evaporation, altered thermal stratification, dissolved-oxygen changes, and consequences for phytoplankton, benthic communities and mobile species [12–16]. Water-quality effects of surface coverings have been demonstrated for artificial monolayers on stored water [17] and metal enrichment has been reported in water bodies hosting PV arrays [18], but chemical release from the modules themselves has received far less attention. The existing leaching literature is dominated by laboratory tests of end-of-life modules using aggressive waste-characterization protocols (crushed fragments, acidic extractants, tumble agitation), which are more severe than realistic field contact [19,20]. Long-term immersion studies of module pieces in pH-adjusted solutions have shown that metals can be released over years, and that release depends strongly on solution chemistry and on cut or damaged edges [21,22]. For crystalline-silicon modules specifically, the first aquatic-toxicity study of component leachates identified Al and Ag as the primary ecotoxicological suspects, with toxicity strongly dependent on module and component type [23]. To our knowledge, no study has yet quantified metal release from intact commercial crystalline-silicon modules under outdoor, natural-temperature water immersion, and no empirical assessment exists for the canal-top PV configuration over drinking-water transfer channels. This study was designed to address the deficiency.

Here we report two outdoor static-immersion campaigns using commercial crystalline-silicon modules (LONGi P-type, TOPCon and IBC; CHINT TOPCon) in Beijing, China: an 8-day autumn campaign comparing intact and broken modules, and a 66-day spring campaign comparing four damage-severity levels plus an IBC broken module. The specific objectives were to (i) characterize the time-resolved release of metals and phenol from modules under conditions representative of a canal-top deployment; (ii) compare intact and damaged modules; (iii) screen all measured concentrations against the Chinese drinking-water standard GB 5749-2022 [24] and the surface-water standard GB 3838-2002; (iv) scale the measured release fluxes to a real transfer canal to assess the water-quality risk of PV corridor deployment; and (v) document in situ water-quality parameters (water temperature, dissolved oxygen, electrical conductivity and turbidity) alongside metal release.

2. Materials and Methods

2.1. Module Materials and Experimental Design

Two campaigns were conducted using tap water in open pools under natural outdoor conditions (Figure A1). In the autumn campaign (Phase 1; 11–19 September 2025; 0–192 h), six pools received one full-size module each: LONGi P-type (PERC), N-type TOPCon and interdigitated back-contact (IBC) modules, each in an intact and a broken state (treatments 1#–6#; module dimensions 2382 mm × 1134 mm × 30 mm, 33.5 kg). Two additional barrels

filled with the same tap water (CK1, CK2) served as blanks. In the spring campaign (Phase 2; 17 April~22 June 2026; 0–1584 h), five pools received one module each: CHINT N-type TOPCon modules with severe (20% area of the whole module), moderate (10% area) and mild damage (5% area) and an intact module (treatments 1#–4#; 2382 mm × 1134 mm × 30 mm, 31.65 kg, obtained from the project site), plus a broken LONGi IBC module (treatment 5#, 20% of the area). The three damage levels (5%, 10% and 20% of module area) were selected to bracket the severity of mechanically induced damage observable in service from localized impact damage to extensive breakage, and to test whether metal release scales with damaged area. Each treatment consisted of a single pool (one module per pool), i.e., no experimental replication was available. In Phase 2, a tap-water blank pool was prepared alongside the treatment pools but began leaking during the campaign, so no usable blank data were collected after deployment. The pre-deployment (t = 0) sample of each pool therefore serves as the Phase 2 background. The pools were PVC-coated polyester-fabric pools (three-layer structure: PVC sheet/polyester mesh/PVC sheet). All containers were cleaned before use and filled with tap water to the volume (2.6 m × 1.6 m × 0.35 m, 1497.6 L ± 260 L). The modules were then thoroughly immersed statically. Each module was laid horizontally in its pool and fully submerged, so that the entire module surface was in contact with water (both faces ≈5.4 m^2 plus edges), i.e., 100% of the module surface area. Pool volume and water depth are listed in Appendix A, Table A1.

Module bills of materials (vendor material declarations) place the Cu-bearing components outside the laminate: the copper ribbons (99.99% Cu; Ag 0.0014%), the junction-box body (PPE 66.8%, Cu 24.2%, Sn 3.3%, Pb 1.9%), the connectors (PPE 55.6%, PA66 27.2%, Cu 11.5%, stainless steel 1.4%) and the cables (XLPE 54%, Cu 46%). The aluminum frame (7.7% of module mass) is a 6005 Al–Mg–Si alloy containing 0.35% Fe, 0.1% Cu, 0.1% Mn and 0.1% Zn; the tempered front glass (80.6% of module mass) contains 0.015% Fe_2O_3 and 0.159% of the Sb_2O_3 fining agent, and the EVA/POE encapsulants (85–95% copolymer) contain 1–5% antioxidant additives. The modules comply with the EU RoHS and REACH regulations, and the LONGi modules passed the Korean KSC 8561 certification, which includes a tap-water leaching test of the module against Article 24 of the Korean Water Supply Act.

2.2. Sampling and Analytical Methods

In Phase 1, water samples were collected at t = 0, 1, 2, 4, 6, 12, 24, 48, 72, 96, 144 and 192 h (12 events); in Phase 2, at t = 0, 1, 2, 4, 10, 24, 48, 72, 96, 144, 192, 240, 288, 336, 408, 576, 744, 912, 1080, 1248, 1416 and 1584 h (22 events). In Phase 1, samples were analyzed for Pb, Cd, As, Ni and phenol; in Phase 2, for Cu, Fe, Mn, Zn, Pb, Cd, Cr(VI), As, Hg and Ni (Appendix A, Table A2). Metals were determined by inductively coupled plasma–mass spectrometry (HJ 700-2014); total Hg by cold-vapor atomic absorption spectrophotometry (HJ 597-2011); Cr(VI) by 1,5-diphenylcarbohydrazide spectrophotometric method (GB/T 7467-87); and phenol by continuous flow analysis spectrophotometry (SL/T 788-2019). In situ water-quality parameters (water temperature, electrical conductivity, dissolved oxygen, turbidity and total dissolved solids) were recorded at each sampling with a portable multiparameter water-quality meter (ProDSS, YSI, Yellow Springs, OH, USA). Detection limits for each analyte are summarized in Appendix A, Table A2. The analyte set covers the metals regulated by GB 5749-2022 and GB 3838-2002 that occur in the module bill of materials (Cu, Fe, Mn, Zn, Ni, Pb, Cd, Hg and Cr(VI)); the selection was driven primarily by the water-quality indicators regulated in GB 3838-2002, combined with the chemical characteristics of the photovoltaic module materials. Phenol was added because it is a regulated priority pollutant in GB 3838-2002 and would indicate leaching of aromatic organics from module polymers. The Phase 1 subset targeted the more toxic elements (Pb, Cd, As), Ni (from stainless-steel

connector parts) and phenol. The full time series of all measured concentrations and in situ parameters are provided in the Supplementary Materials (Tables S1 and S2).

2.3. Data Processing: Mass Balance and Release Rates

To account for rainfall dilution and evaporative concentration during the outdoor campaign, the water volume of each pool at each sampling was reconstructed as:

$$V = V1 + V2 - V3 \quad (1)$$

where $V1$ is the initial water volume, $V2$ the cumulative precipitation volume and $V3$ the cumulative evaporation volume between deployment and sampling. Precipitation was taken from the Beijing Water Authority rain-gauge network for the experimental site (https://nsbd.swj.beijing.gov.cn/csyq1.html, accessed on 30 July 2026), and evaporation was estimated from the mean daily evaporation of Beijing (annual mean 1842.2 mm, i.e., 5.05 mm/d, from the National Earth System Science Data Center, https://www.data.ac.cn/), multiplied by the pool surface area (2.6 m × 1.6 m). The leached mass M (mg) of each element in each pool was then computed as:

$$M = V \times C \quad (2)$$

where C (mg/m^3) is the measured concentration. Note that M is the instantaneous net pool burden (released minus re-adsorbed/precipitated mass). For the elements with strong re-adsorption (notably Fe), the true cumulative release exceeds the net mass, so the masses and rates reported here are conservative. Release rates v (mg/h) between consecutive samplings were computed as:

$$v = (M2 - M1)/(t2 - t1) \quad (3)$$

where subscripts 1 and 2 denote consecutive sampling events. Background (blank) concentrations were used to distinguish true module-derived release from the tap-water background: the CK1/CK2 barrels in Phase 1 and the t = 0 samples of each pool in Phase 2 (the Phase 2 blank pool leaked during the campaign). Concentrations below the limit of detection (LOD) were treated as zero for mass and rate calculations.

The measured concentration C in Equation (2) is used without subtracting the initial background, so the reported masses include the initial background mass. The background-corrected burden is M′ = V × (C − C0), where C0 is the measured t = 0 concentration of the same pool (Phase 2) or the mean blank concentration (Phase 1). As a worked example, at the Cu peak (pool 4#, t = 408 h) C = 105.0 µg/L and C0 = 1.0 µg/L (Table S2), so C − C0 = 104.0 µg/L and the initial background accounts for only 1.0/105.0 ≈ 1% of the reported burden. At t = 24 h (C = 5.2 µg/L) the corresponding share is ≈19%, which is why M uses the measured concentration. Release rates between consecutive samplings (Equation (3)) are only weakly affected by this constant background, because it enters the difference (M2 − M1) only through the reconstructed volume change between the two samplings.

2.4. Water-Quality Benchmarks and Risk Screening

Measured concentrations were screened against the limit values of the Chinese Standards for Drinking Water Quality (GB 5749-2022), the Environmental Quality Standards for Surface Water (GB 3838-2002), and, for health context, the WHO Guidelines for Drinking-water Quality [25,26] and the EU Drinking Water Directive [27]. Hazard quotients were computed as

$$HQ = C/Cst \quad (4)$$

where Cst is the standard limit values for each detected element [28,29]. HQ as used here is a concentration-to-standard ratio, i.e., a screening-level regulatory benchmark comparison. It

is not a complete human-health risk assessment, which would additionally require exposure parameters such as ingestion rate and body weight. To scale the observed release to a real canal-top deployment, the per-module daily release flux from Phase 2 was combined with the design discharge of the LDWTP canal (350 m^3/s; planned annual diversion of 9.5 km^3) [30] to estimate the steady-state concentration increment as

$$\Delta C = (n \times L \times F)/Q \quad (5)$$

where n is the number of modules per unit canal length, L the corridor length considered (km), F the per-module release flux (mg/d) and Q the canal discharge (m^3/d). Equation (5) is a screening-level steady-state dilution calculation that assumes complete mixing of the released flux across the full canal cross-section and does not resolve hydrodynamic dispersion or transport processes. The resulting increments are therefore order-of-magnitude screening estimates rather than transport-model predictions.

2.5. AI Tool Disclosure

DeepSeek (V4) was used exclusively as a programming aid to debug Python (version 3.12) scripts for data processing and to draw graphics; it was not used in the experimental design, data collection or data analysis. All analyses were conducted and verified by the authors, who take full responsibility for the content.

3. Results

3.1. Phase 1 (Autumn, 8-Day Immersion): Concentration Time Series

Water temperature declined from 27.9–31.8 °C to 19.1–22.0 °C over the 8-day campaign. Dissolved oxygen remained near saturation (6.6–8.5 mg/L), electrical conductivity was 313–444 µS/cm, total dissolved solids were 220–265 mg/L and turbidity stayed ≤3 NTU throughout (Table S1), indicating well-oxygenated, mildly mineralized water with little suspended matter. Among the five target analytes, only As and Ni were consistently detected. Arsenic (As) concentrations ranged from 0.24 to 0.35 µg/L across all treatments and remained essentially constant over time, with no systematic difference among module types or between intact and broken modules (Table 1; the time series are shown in Figure 1 and Table S1). The blank barrels contained 0.22–0.32 µg/L As, indicating that most of the measured As was tap-water background and that the module-derived increment was ≤0.1 µg/L. Nickel (Ni) increased gradually in the broken P-type pool (2#) and the N-type TOPCon pools (3# intact and 4# broken), from 0.73 to 1.69 µg/L, 0.74 to 2.60 µg/L and 0.87 to 2.48 µg/L, respectively, by t = 192 h, while the intact P-type, IBC and blank pools remained below 0.7 µg/L. Lead (Pb) was detected sporadically at 0.11–0.57 µg/L in a few samples, Cd was detected once (0.08 µg/L) and phenol was detected at 0.43–0.50 µg/L in a few samples, all near the method detection limits and without temporal trends; the overwhelming majority of samples were below detection. Release rates of As (−0.03 to 0.04 µg/(L·h)) and Ni (−0.04 to 0.11 µg/(L·h)) were maximal in the first 12 h; thereafter, As rates were indistinguishable from zero, whereas small but persistent positive Ni rates (≤0.01 µg/(L·h)) sustained the gradual Ni increase in pools 2#–4#. Rates were only marginally higher in broken than in intact modules.

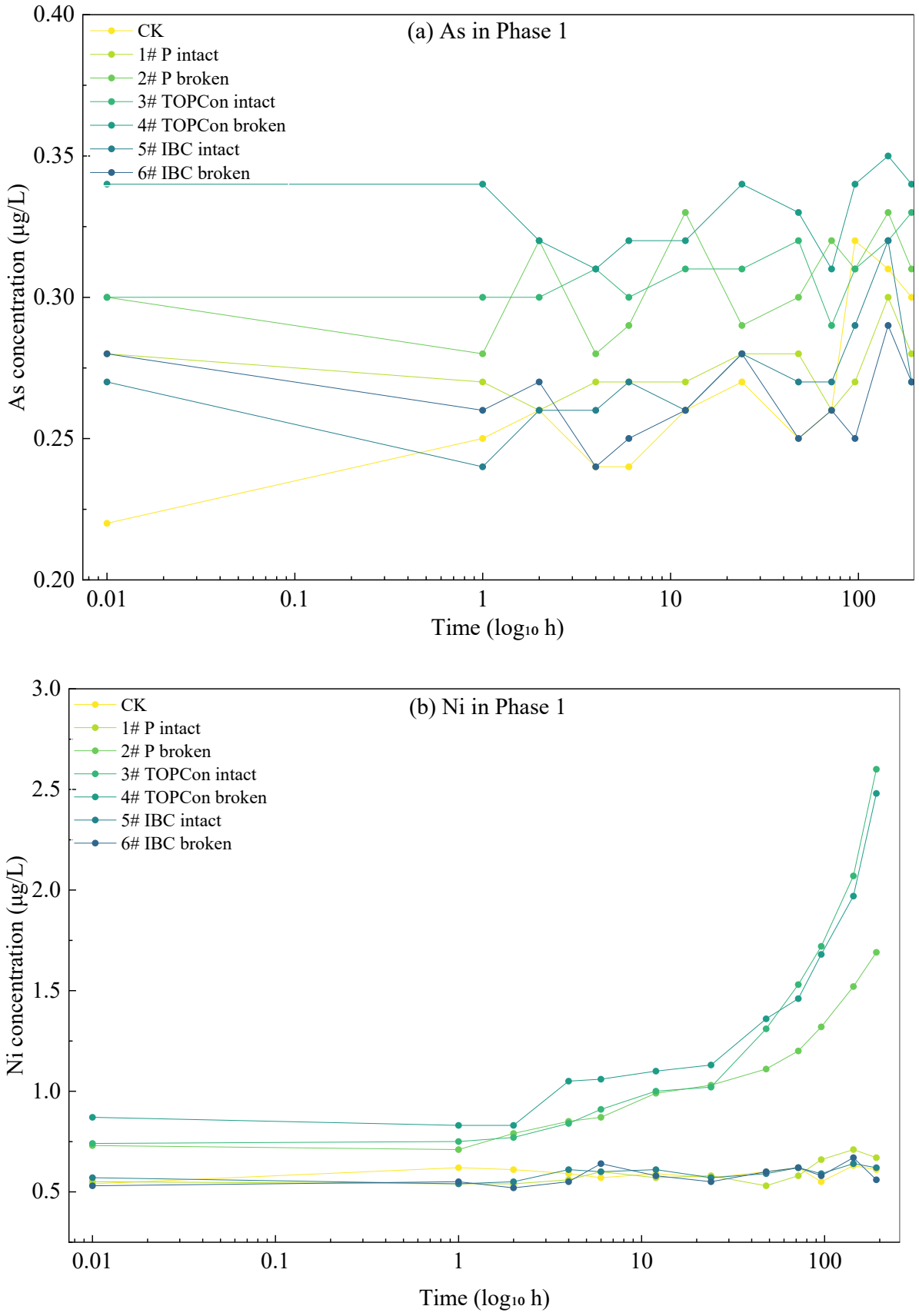


Figure 1. Time series of As and Ni concentrations (μg/L) during Phase 1 (autumn, 0–192 h).

Table 1. Phase 1 (autumn): Summary of measured concentrations vs. benchmarks.

Analyte	Detection	Range Across Pools (μg/L)	Blank (μg/L)	Max HQ vs. GB 5749-2022	Max HQ vs. GB 3838-2002 Class I
As	all samples	0.24–0.35	0.22–0.32	0.035	0.007
Ni	all samples	0.53–2.60	0.54–0.63	0.13	/
Pb	sporadic	0.11–0.57	mostly <LOD	0.057	0.057
Cd	once (t = 4 h)	0.08	<LOD	0.016	0.08
Phenol	sporadic	0.43–0.50	mostly <LOD	/	0.25

3.2. Phase 2 (Spring, 66-Day Immersion): Concentration Time Series

Water temperature rose from 16.7–18.5 °C to 26.8–33.3 °C over the campaign. Dissolved oxygen remained high (6.0–10.1 mg/L), and electrical conductivity and total dissolved solids rose from ~360–400 μS/cm and ~270–290 mg/L at deployment to 415–591 μS/cm and up to 347 mg/L, tracking the evaporative concentration of the pools; turbidity stayed below 1.2 NTU (Table S2). Of the ten metals, Cu, Fe, Mn, Zn, As and Ni were detected in all pools, Pb was detected sporadically and only in the severely damaged pool (1#), whereas Cd, Cr(VI) and Hg remained below their detection limits (Table 2; the time series are shown in Figure 2 and Table S2). Copper (Cu) showed the largest release, increasing from a pre-deployment background of 0.61–1.43 μg/L to maxima of 53.4–105.0 μg/L between 336 and 408 h (14–17 d), with the highest value in the intact-module pool (4#, 105.0 μg/L), followed by moderate damage (10% area, 2#, 60.9 μg/L), severe damage (20% area, 1#, 58.5 μg/L), mild damage (5% area, 3#, 53.4 μg/L) and the broken IBC module (5#, 33.1 μg/L). Given the absence of a concurrent Phase 2 blank, these increases are attributed primarily to the modules; a minor contribution from unrecognized background sources cannot be fully excluded (Sections 2.3 and 4.5).

Table 2. Phase 2 (spring): Concentration ranges and peaks of the ten metals.

Analyte	Background t = 0 (μg/L)	Range Across Pools (μg/L)	Peak (μg/L; Pool; Time)	Max HQ vs. GB 5749-2022	Max HQ vs. GB 3838-2002 Class I
Cu	0.61–1.43	0.91–105.01	105.01 (4#; 408 h)	0.11	>Class I (10 μg/L) in all pools 72–1248 h; <Class II
Fe	<0.82–43.54	<0.82–48.12	48.12 (2#; 24 h)	0.16	below
Mn	0.92–3.36	0.45–6.56	6.56 (2#; 96 h)	0.07	below
Zn	2.91–4.78	0.97–5.94	5.94 (1#; 72 h)	<0.01	below (limit 0.05 mg/L)
As	0.43–0.49	0.35–1.01	1.01 (5#; 96 h)	0.10	below
Ni	0.54–0.60	0.54–2.35	2.35 (4#; 576 h)	0.12	below
Pb	<0.09	<0.09–0.16 (1# only)	0.16 (1#; 144 h)	below	below
Cd	<0.05	<0.05	<0.05	below	below
Cr(VI)	<LOD	<LOD	<LOD	below	below
Hg	<0.04	<0.04	<0.04	below	below

Iron (Fe) concentrations fluctuated strongly in the first 6 d (max 48.1 μg/L in pool 2# at 24 h) and then declined to 2.7–3.3 μg/L by the end of the campaign. Manganese (Mn) reached 6.6 μg/L (pool 2# at 96 h) and Zn, As and Ni peaked at 5.9, 1.0 and 2.4 μg/L, respectively (pool 1#, pool 5# and pool 4#). Zinc concentrations fell below the LOD in most pools after ~45 d. All detected concentrations remained at least one to three orders of magnitude below the GB 5749-2022 drinking-water limits, with the single exception of Cu relative to the GB 3838-2002 Class I limit: Cu exceeded the 10 μg/L Class I limit in all pools from 72 h until 1248 h (52 d), but remained below 1000 μg/L, the Class II limit, as well as the drinking-water limit.

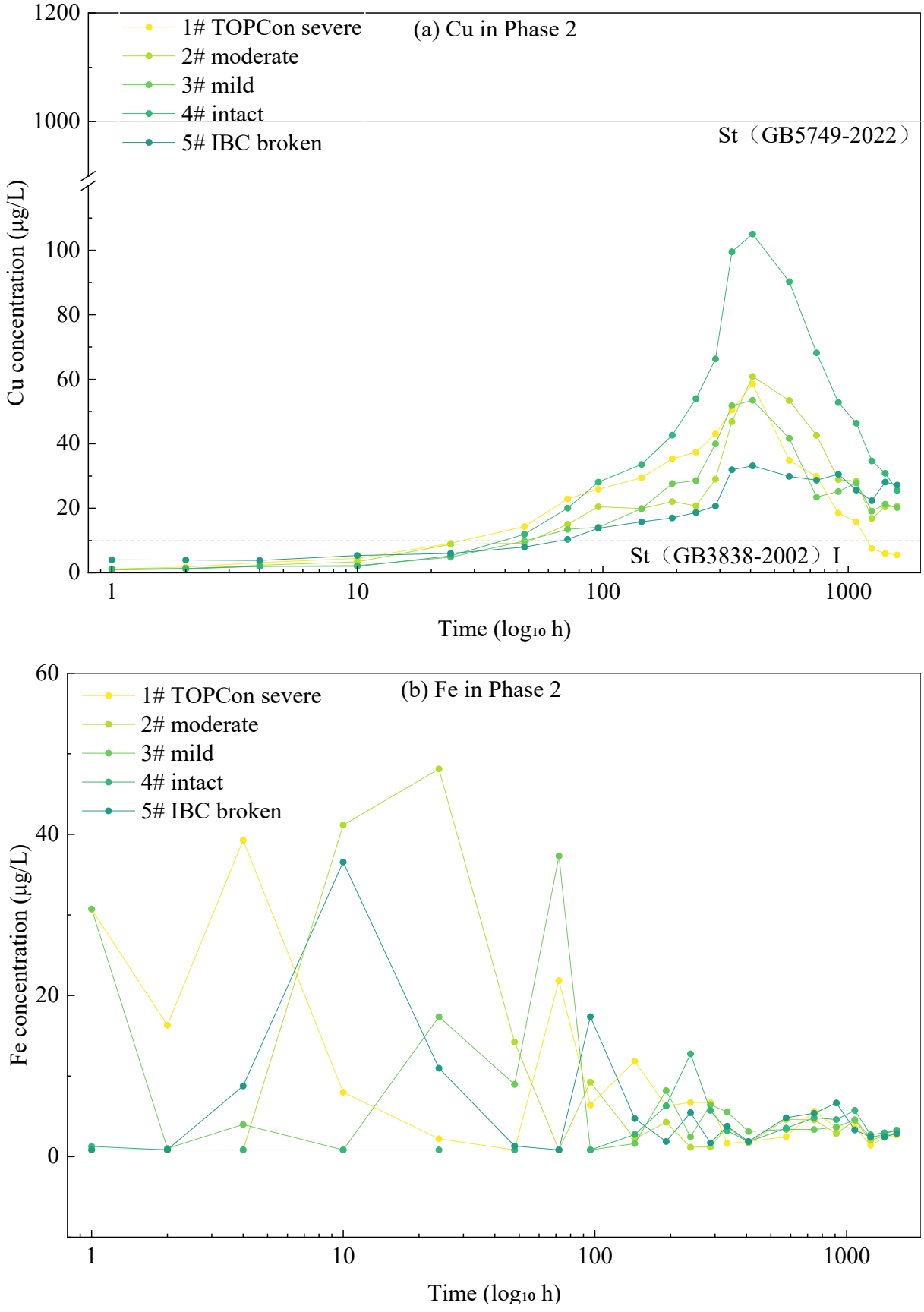


Figure 2. *Cont*.

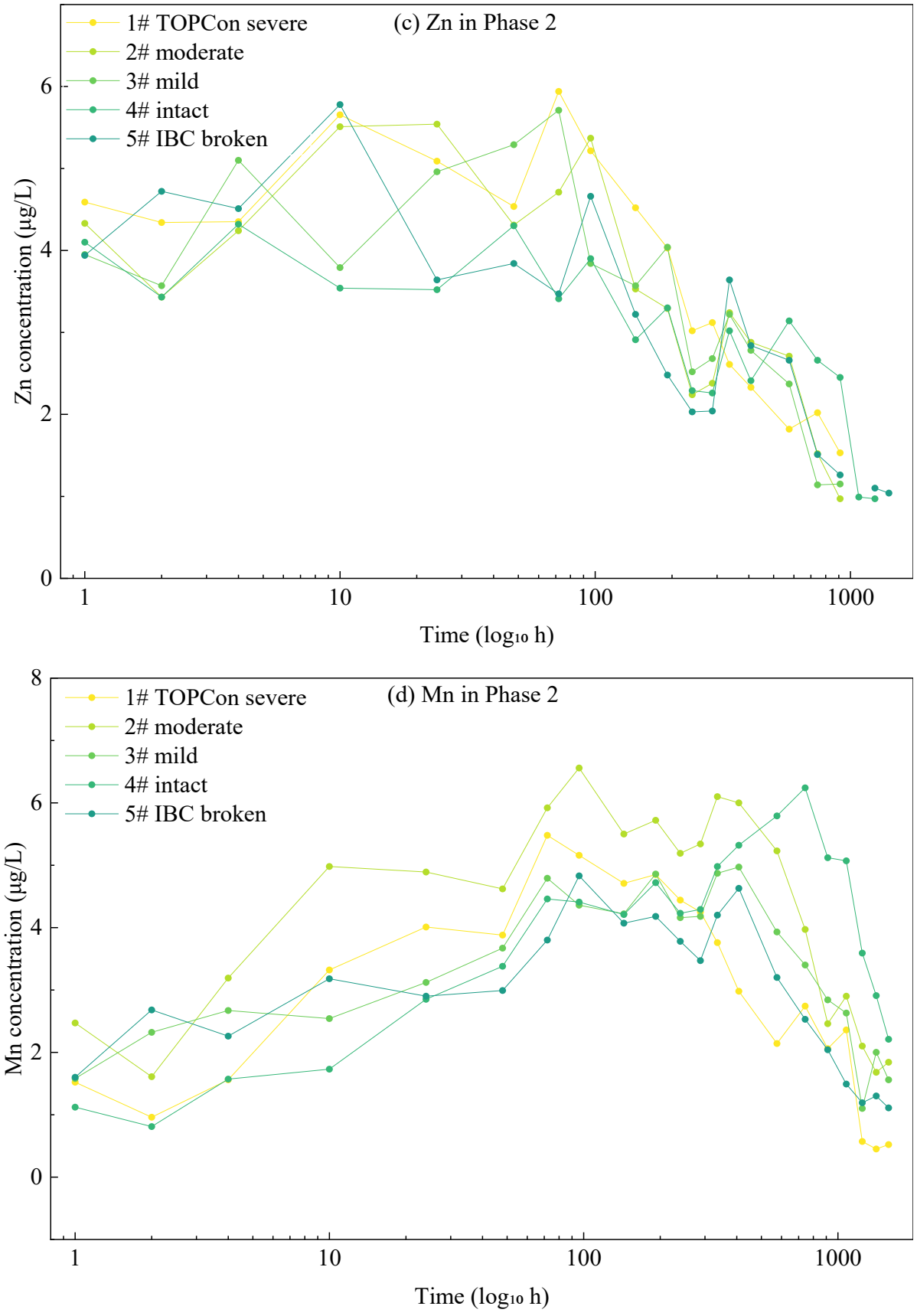


Figure 2. *Cont*.

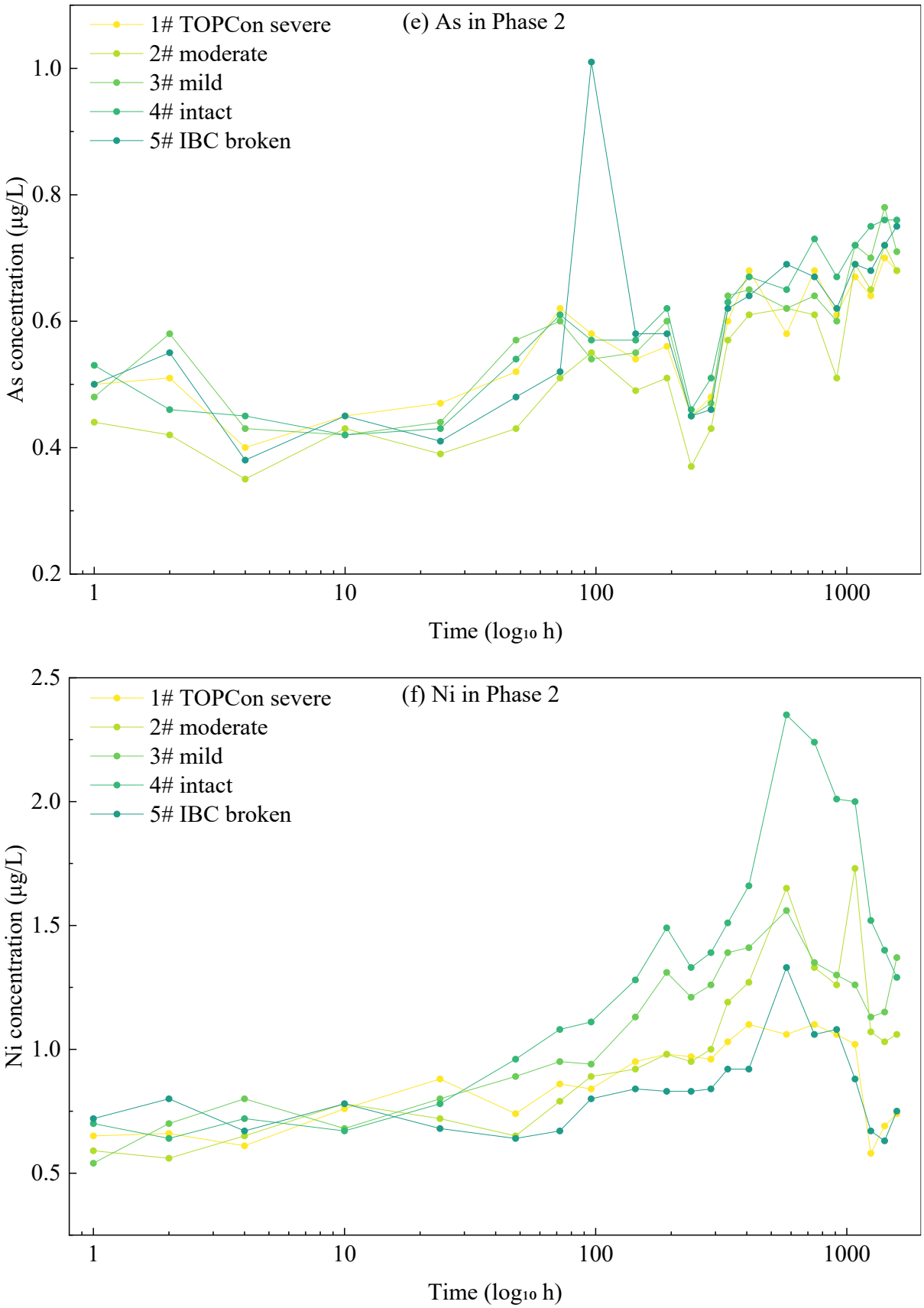


Figure 2. Time series of Cu, Fe, Mn, Zn, As and Ni concentrations (μg/L) during Phase 2 (spring, 0–1584 h).

3.3. Phase 2: Leached Masses and Release Rates

After correction for rainfall and evaporation, the instantaneous net leached masses per pool ranged over 1.52–89.07 mg (Fe), 0.83–12.54 mg (Mn), 1.17–194.5 mg (Cu), 1.24–11.01 mg (Zn), 0.67–1.87 mg (As) and 1.03–4.50 mg (Ni) (Table 3). These masses are the net pool burdens at each sampling, i.e., the standing dissolved mass available in the pool water, rather than cumulative releases. The quantity a downstream water body would actually receive additionally depends on the exchange and flushing between the corridor and the canal, which the batch pools do not reproduce. In detail, for Fe, whose net rates oscillate strongly (Table 3), the true cumulative release can substantially exceed the net mass. Copper and iron dominated the mass release, whereas As and Ni were the smallest. The mass release trajectories showed an initial pulse followed by decline or stabilization for all elements except Cu, whose mass continued to increase into the mid-campaign (peak at 400–800 h). Release rates were highest in the first 4 d: Fe oscillated between −81.6 and +57.1 mg/h during the first 48 h (a release-re-adsorption pattern), and Mn, Zn and As rates converged to near-zero within 24–144 h; Ni rates likewise converged within ~24 h in most pools, although Ni concentrations in the intact-module pool (4#) continued a slow increase to a maximum of 2.35 μg/L at 576 h (Table 2). Copper was the only element with a pronounced secondary-release phase (up to 1.28 mg/h at 8–17 d) and the longest active period, stabilizing only after ~576 h (24 d). Across the five single-pool treatments, the rate ranges of Fe, Mn and Cu were widest in pool 5# (broken IBC); for Zn it was in pool 1# (severe damage, 20% area) and for As and Ni it was in pool 3# (mild damage, 5% area). As descriptive observations from unreplicated pools, these patterns cannot be separated from pool-specific variability, but they are consistent with element-specific release dynamics not being monotonically controlled by damage severity.

Table 3. Phase 2 (spring): Net leached masses, rate ranges and stabilization times.

Analyte	Net Mass Range Across Pools (mg)	Max Net Mass (mg; Pool)	Rate Range (mg/h)	Stabilization Time
Fe	1.52–89.07	89.07 (1#)	−81.59 to 57.05	~144 h (6 d)
Mn	0.83–12.54	12.54 (4#)	−2.62 to 2.06	~48–144 h
Cu	1.17–194.50	194.50 (4#)	−0.26 to 4.81 (secondary peak 1.28 at 8–17 d)	~576 h (24 d)
Zn	1.24–11.01	11.01 (1#)	−1.72 to 3.21	~48–144 h
As	0.67–1.87	1.87 (5#)	−0.16 to 0.19	~24 h
Ni	1.03–4.50	4.50 (4#)	−0.12 to 0.31	~24 h (most pools); 576 h (4#)

Note: Masses are instantaneous net pool burdens (M = V × C); where re-adsorption occurs (notably Fe), the true cumulative release may exceed the net mass.

3.4. Compliance Screening and Screening-Level Hazard Quotients

All measured concentrations in both campaigns met the GB 5749-2022 drinking-water limits and the GB 3838-2002 Class II limits (Tables 1 and 2). The maximum hazard quotient (HQ = C/Cst, limit against GB 5749-2022) was 0.11 for Cu (105.0 μg/L vs. 1000 μg/L), 0.16 for Fe (48.1 μg/L vs. 300 μg/L), 0.07 for Mn, 0.12 for Ni (against the 20 μg/L expanded-index limit), 0.10 for As, and <0.01 for Zn. Against the stricter Class I surface-water limits, only Cu exceeded the benchmark (HQ up to 10.5 against the 10 μg/L Class I limit), whereas all other elements remained below.

Using the campaign-average per-module daily Cu release of ~2.9 mg/d (194.5 mg over 66 d) and assuming a dense corridor configuration of 1000 modules over a 1 km corridor length (L = 1 km in Equation (5)), the expected steady-state Cu increment at the LDWTP design discharge of 350 m^3/s is 0.97×10^{-4} μg/L, i.e., ~10^{-5} of the Class I limit and ~10^{-7}

of the drinking-water limit; the corresponding increments for all other elements are even smaller. Under the maximum observed interval-rate scenario (4.81 mg/h, i.e., 115 mg/d; Table 3), the increment is 3.8×10^{-3} µg/L, i.e., ~4×10^{-4} of the Class I limit and ~4×10^{-6} of the drinking-water limit. These increments scale linearly with the assumed corridor length (Equation (5)): a 10 km corridor would contribute ~4×10^{-2} µg/L of Cu under the maximum observed interval-rate scenario, still ~0.4% of the Class I limit. Higher transient release rates than the maximum observed interval value cannot be excluded; cumulative metal release from materials placed in water engineering works is assessed at the system scale over the service life [31].

4. Discussion

4.1. Element Sources in Module Materials

The observed release pattern is consistent with the material composition of crystalline-silicon modules [32,33]. Copper, the dominant leached element, is abundant in the copper ribbons (99.99% Cu; Ag 0.0014%), the junction-box body (~24.2% Cu), connectors (~11.5%) and cables (~46%)—components that are located at the module edges and back side, outside the glass/EVA encapsulation, and are therefore directly exposed to water and electrochemically active. Iron, Mn and Zn originate from the aluminum frame alloy (6005 Al–Mg–Si: 0.35% Fe, 0.1% Cu, 0.1% Mn, 0.1% Zn) and, for Fe, the glass (0.015% Fe_2O_3); the frame constitutes the outermost, permanently wetted metallic surface, which explains the early Fe pulse. Nickel is present only at trace level in the copper ribbon (<0.0001%) and in the stainless-steel parts of the connectors (1.4%), the latter being its more plausible source. As in both campaigns remained essentially at the tap-water background level (blank barrels 0.22–0.32 µg/L, module-derived increment ≤0.1 µg/L); thus, the trace As detected is attributed to the source water rather than to the modules. Pb is present as a minor constituent (1.9%) of the junction-box body, most plausibly in its Sn-Pb solder contacts, but remains encapsulated inside the box, consistent with its sporadic near-LOD detection in the severely damaged pool (1#); Cd and Hg are essentially absent from the bill of materials of modern crystalline-silicon modules [34], and phenol has no major source in module polymers (EVA, POE, PET/PVDF backsheets, PPO junction boxes; the 1–5% antioxidant additives of the encapsulants are strongly partitioned into the polymer matrix), consistent with its sporadic near-LOD detections and with the expectation that encapsulant degradation products are primarily acetic acid and ketones rather than phenols [35].

4.2. Release Dynamics: Initial Pulse, Re-Adsorption, and the Delayed Cu Release

A two-stage kinetic signature was observed here: a fast initial release (0–4 d) followed by near-zero net rates is consistent with a two-stage process. The loosely bound surface species (frame oxide films, flux residues, particles deposited during manufacturing) dissolve rapidly, after which the solution approaches pseudo-equilibrium between the module surfaces, corrosion products and suspended/adsorbed phases. The oscillating Fe fluxes in the first 48 h indicate concurrent release and re-adsorption onto module surfaces and pool walls. The unique behavior of Cu, slow build-up, a secondary-release peak at 8–17 d and stabilization only after 24 d, is best explained by the progressive breakdown of surface passivation on the exposed Cu parts (junction box, connectors, cables, ribbon edges) driven by dissolved oxygen in the mildly mineralized tap water (electrical conductivity 313–591 µS/cm; Tables S1 and S2), i.e., a corrosion-controlled rather than dissolution-controlled regime [36,37]. This interpretation aligns with the finding that aqueous leaching of modules proceeds preferentially via "weak spots" and exposed internal layers [22] and with the dominance of junction-box/cable leachates in the c-Si aquatic-toxicity screening of Tavolacci et al. [23].

These observations can be organized into a proposed conceptual two-stage release model (Figure 3). Stage 1 (0–4 d) is surface-controlled: weakly bound species (frame oxide films, flux residues, manufacturing dust) dissolve or desorb, producing the early Fe/Mn/Zn pulse and the initial Cu rise; the strong Fe oscillation (−81.6 to +57.1 mg/h within the first 48 h) reflects concurrent release and re-adsorption, most plausibly precipitation as Fe oxyhydroxides that also scavenge other trace metals. Stage 2 is corrosion-controlled and element-selective: only Cu sustained a pronounced delayed release peak at 8–17 d. In the intact-module pool (4#), the apparent Cu release rate accelerated from ~0.28 µg/(L·h) over the first 96 h to ~0.69 µg/(L·h) between 288 and 336 h (12–14 d), and declined after the 408 h maximum. The delay before the secondary peak is consistent with the time required for: (i) moisture ingress through the cable insulation and junction-box seals [38]; (ii) breakdown of the air-formed oxide film on the Cu surfaces in oxygenated, aided-by-alkali leaching from the soda–lime glass (13.9% Na_2O) and by local acidification from acetic acid released during EVA hydrolysis [35], which destabilizes protective cuprous-oxide/carbonate films; and (iii) galvanic coupling with the Al frame, which is anodic to Cu: the frame corrodes first (the early Fe pulse) while protecting the Cu parts, and once the frame surface passivates the corrosion load shifts to Cu, a sequence that naturally produces a delayed Cu peak. Stabilization after ~24 d then reflects re-passivation by precipitated copper carbonates and co-precipitation with Fe oxyhydroxides. Because release is governed by water chemistry and the electrochemical state of the exposed parts rather than by bulk composition alone [39,40], single 24–48 h laboratory leach tests cannot capture this delayed phase and may substantially underestimate Cu release in long-term contact [21,22]. Alternative explanations for the delayed Cu peak are acknowledged: reversible desorption of Cu from Fe oxyhydroxides as water chemistry drifted, microbial uptake and release, or localized pitting at manufacturing defects could each produce a secondary concentration maximum without galvanic coupling with the frame. The galvanic sequence is preferred because it directly explains the observed order of events (an early Fe pulse from the frame, followed by Cu release once the frame passivates), but it remains a clearly hypothetical mechanism: no direct electrochemical measurements (open-circuit potentials, corrosion currents) were performed and pH was not monitored (Section 4.5), so this explanation should be regarded as a working hypothesis; direct electrochemical monitoring and pH records should test it in future work.

4.3. Seasonal and Damage Effects

The autumn and spring campaigns spanned comparable water temperatures (autumn 19.1–31.8 °C; spring 16.7–33.3 °C), yet the As stabilization time was slightly longer in spring (24 h vs. 12 h), and Ni, which rose gradually over the full 8 d autumn campaign without reaching a plateau, converged to near-zero net rates within ~24 h in most spring pools, with a slow continued increase in the intact-module pool to a peak at 576 h (Table 2); the rate ranges of both elements were marginally wider (As: −0.03 to 0.04 vs. −0.08 to 0.05 µg/(L·h); Ni: −0.04 to 0.11 vs. −0.06 to 0.12 µg/(L·h), consistent with modest temperature control on early dissolution kinetics. In the single pools tested, the intact-module pool showed the highest Cu, Mn and Ni release, whereas the severely damaged pool (20% area) showed the highest Fe and Zn release; because each treatment comprised only one pool, these patterns are descriptive observations that cannot be separated from pool-specific variability and are not established treatment effects. The absence of a monotonic damage–release relationship is nonetheless an important and somewhat counterintuitive result. It suggests that, for edge-mounted metal components, corrosion is controlled more by the electrochemical microenvironment (oxygen supply, local pH, galvanic coupling, accumulation of corrosion products) than by the gross cracked area of the laminate; broken glass surfaces may even act as sorption sites that scavenge released metals. From a management perspective, these

observations suggest that even intact modules should be covered by any water-quality monitoring program, not only broken ones.

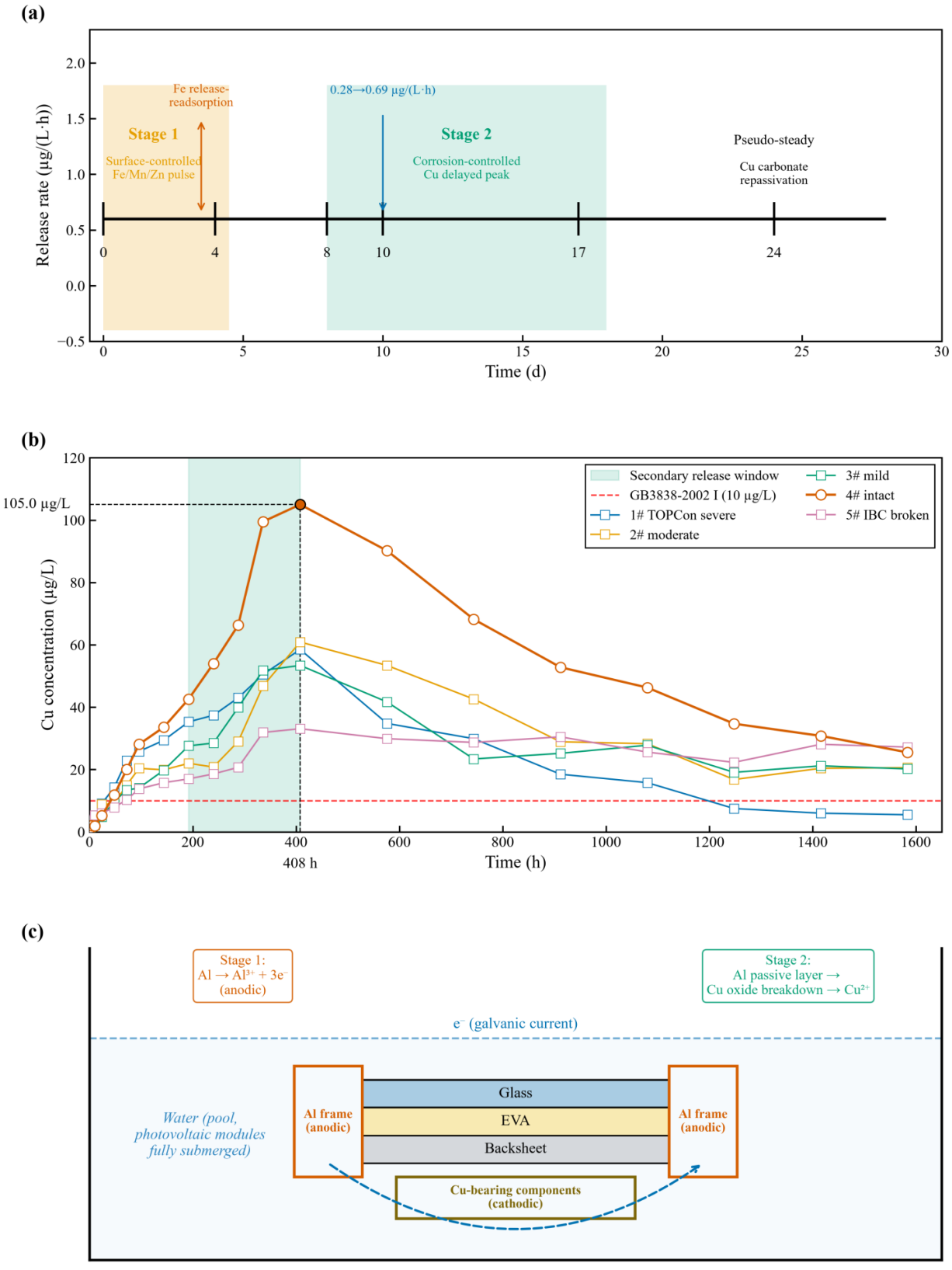


Figure 3. Proposed conceptual two-stage release model for submerged crystalline-silicon photovoltaic modules. (**a**) Stage 1 (0–4 d): Surface-controlled dissolution and desorption of oxide films and manufacturing residues, producing the early Fe/Mn/Zn pulse with Fe release–re-adsorption

oscillations. (**b**) Stage 2 (8–17 d): Corrosion-controlled delayed Cu release after breakdown of the passivation film on the Cu-bearing components; the Cu concentration time series of the intact-module pool (4#) shows the secondary-release window (shaded green) and the GB 3838-2002 Class I limit of 10 μg/L (red dashed line), with a peak concentration of 105.0 μg/L at 408 h. (**c**) Schematic of the hypothesized galvanic coupling between the Al frame (anodic) and the Cu-bearing components (cathodic) in a fully submerged module cross-section (glass/EVA/backsheet, Al frames on both sides, and Cu components on the rear side). Stage 1: Al frame dissolves anodically ($Al \rightarrow Al^{3+} + 3e^-$), generating a cathodic protection current that suppresses Cu release. Stage 2: After Al surface passivation, the corrosion load shifts to Cu, leading to oxide film breakdown and delayed Cu^{2+} release. e^-, electron; EVA, ethylene–vinyl acetate.

4.4. Scaling to a Real Transfer Canal and Implications for PV Corridors

The observed pool concentrations arise from a "near-stagnant, small-volume" batch configuration, which is expected to be conservative for concentration; a real transfer canal continuously renews the water. Two properties of the design make the pools conservative in concentration: stagnation eliminates advective dilution for a given release flux, and full submersion maximizes the wetted module area (≈5.4 m^2, both faces), whereas canal-top modules would be wetted only intermittently. Two countervailing effects are also acknowledged: flowing canal water renews dissolved oxygen, which can accelerate corrosion-controlled release, and canal water chemistry differs from tap water; for the tested stagnant, fully submerged conditions, the screening is therefore expected to be conservative for concentration, but this does not extend to the release flux. The transfer canal conveys a design discharge of 350 m^3/s (planned annual diversion of 9.5 km^3) [30], so the concentration increment contributed by even a dense PV corridor (~1000 modules/km, evaluated over a 1 km corridor length, L = 1 km in Equation (5)) is of the order of 10^{-4} μg/L for Cu and far less for the other elements based on the campaign-average release rate; substituting instead the maximum observed interval release rate (4.81 mg/h, i.e., 115 mg/d) leaves the Cu increment at ~3.8×10^{-3} μg/L, still more than three orders of magnitude below the most stringent regulatory benchmark considered here (GB 3838-2002 Class I Cu limit, 10 μg/L); because the increment scales linearly with the assumed corridor length (Equation (5)), a 10 km corridor would contribute ~4×10^{-2} μg/L of Cu under the maximum observed interval-rate scenario, still <1% of the Class I limit. This screening result is consistent with the dedicated 1-D hydrodynamic water-quality simulations of the project report; such a one-dimensional Saint-Venant modeling is established practice for this canal [41]. Because Equation (5) assumes complete mixing and does not resolve hydrodynamic dispersion or transport losses, these increments remain screening-level estimates to be validated against field monitoring once pilot corridors are built (Section 4.5). The Cu exceedance of the Class I limit observed in the pools is therefore attributable to the batch configuration and would not be expected in the flowing canal under normal operation, where continuous advective dilution keeps the estimated increment orders of magnitude below the limit; however, this extrapolation remains a screening estimate (Equation (5)) that has not yet been verified by field monitoring, and elevated local concentrations in stagnant or poorly mixed canal sections cannot be excluded. Nevertheless, Cu warrants attention for two reasons: it was the only element to approach any benchmark in the experiments, and the canal baseline study of Guo et al. [11] estimated that Cu could affect 8.5% of the algal community even at current background levels, so additional Cu inputs should be minimized. Practical measures follow directly: (i) specify junction boxes, connectors and cables with water-contact-compatible materials or full encapsulation; (ii) promptly remove fallen or broken modules and construction debris; (iii) include Cu, As and Ni in the routine monitoring program of canal-top PV sections [42]; and (iv) locate PV support structures outside the wetted perimeter where possible so that only panel undersides are near the water surface [5]. Module-level evidence

points the same way: the LONGi modules used in this study passed the Korean KSC 8561 certification, which includes a tap-water leaching test of the module against the Korean Water Supply Act, although such certification tests are short-term and would not capture the delayed, corrosion-controlled Cu release identified here.

4.5. Limitations and Future Work

Our experiments used static tap-water pools rather than flowing canal water, a single climatic location, two module suppliers and module models, a single pool per treatment (no experimental replication, so treatment differences cannot be tested statistically; the triplicate analyses are analytical replicates only [43]), and a limited analyte set (metals and phenol; microplastics, acetic acid and other organic degradation products were not measured; only dissolved metals were quantified, so the particulate and colloidal fractions were not separately assessed). Pool volumes are listed in Appendix A, Table A1; the modules were fully submerged (≈5.4 m^2 wetted area per module), enabling area-normalized flux estimates. Batch immersion cannot reproduce advective dilution, but it biases results conservatively (higher concentrations than the field case), which is appropriate for a safety screening. In Phase 2 the tap-water blank pool began leaking during the campaign and had to be abandoned, so no continuous concurrent blank is available. The Phase 1 blank barrels (CK1/CK2), however, showed no metal accumulation over 8 d, suggesting that external inputs (atmospheric deposition, container release) were minor. A sensitivity check bounds the potential Phase 2 background contribution: at the Cu peak the initial (t = 0) background accounts for only ~1% of the pool burden (Section 2.3), and a hypothetical unrecognized background source would have had to supply ≈10 µg/L by day 17 to explain even 10% of the peak Cu (≈0.6 µg/(L·d)), whereas the absence of any detectable accumulation in the Phase 1 blanks bounds an analogous input at <0.006 µg/(L·d) (no measurable change over 8 d at LODs of 0.05–0.35 µg/L), two orders of magnitude lower. The evaporative EC/TDS rise (Section 3.2) is likewise consistent with simple mass conservation. The measured concentration changes are therefore attributed primarily to the modules, although a minor contribution from unrecognized background sources cannot be fully excluded in the absence of a concurrent Phase 2 blank. The multiparameter meter was not equipped with a pH electrode, so pH was not recorded and corrosivity indices (e.g., the Langelier index) could not be computed; the mildly mineralized character of the water is documented instead by electrical conductivity and TDS (Tables S1 and S2). Rainfall was accounted for volumetrically (Equation (1)) but not chemically; rainwater acidity and its influence on metal release from materials [44], as well as UV-driven degradation of encapsulants [35], were not simulated. The PVC-coated polyester-fabric pools could in principle release additives, although the stable blanks argue against a material contribution. The full-submersion configuration is likewise conservative relative to canal-top operation, where modules would contact canal water only intermittently (rainfall, splashing and condensation); thus, for the tested conditions, the measured concentrations are expected to overestimate canal-side concentrations, although this conservatism does not necessarily extend to the release flux (Section 4.4). The immersion durations (8 and 66 d) are short relative to the 25–30-year service life of PV modules; corrosion, material aging, UV exposure and thermal cycling act over years, so the results characterize initial-immersion kinetics and do not quantify lifetime release. This limitation is mitigated by the intended operational regime: canal-top PV corridors will operate under strict online monitoring and maintenance, and a module falling into the canal would be detected and removed promptly, so the tested immersion windows approximate the realistic exposure duration of a fallen module; the results nevertheless characterize the early exposure phase conservatively rather than providing a lifetime-release estimate. Field validation of the canal-scale

screening was not possible at this stage: a ~900 m PV corridor has been operating over the Beijuma River Discharge Channel for more than two years, but no module has fallen into the channel during this period, so no in situ validation opportunity has arisen, and no corridor has yet been built over the main transfer canal itself; the scaling therefore relies on the pool experiments and the project's 1-D hydrodynamic water-quality simulations. The incident-free operating record of the discharge-channel corridor is consistent with the intended operational regime, under which a fallen module would be detected and removed promptly. Future work should (i) repeat the tests in flowing water with canal-representative chemistry; (ii) measure the full spectrum of organic leachates and microplastics; including the particulate and colloidal metal fractions; (iii) verify the 1-D water-quality model against field monitoring once pilot corridors are built; (iv) extend aquatic-ecotoxicity testing of Cu-bearing component leachates in Chinese indicator species, adding Ag and Al to the analyte set, because these elements were identified as the primary ecotoxicological suspects in component leachates [23] and Ag is present in the copper ribbon (0.0014%); and (v) run replicated mesocosms with a continuous blank pool and pH monitoring so that treatment effects can be tested statistically [43].

5. Conclusions

Two outdoor static-immersion campaigns with commercial crystalline-silicon PV modules representative of canal-top deployment over a long-distance water transfer project demonstrated that: (1) only Cu, Fe, Mn, Zn, As and Ni were released at μg/L levels, while Cd, Cr(VI) and Hg remained below detection limits and Pb and phenol were detected only sporadically near their method detection limits; (2) Cu was the dominant leached element (max 105 μg/L), exceeding the GB 3838-2002 Class I benchmark (10 μg/L) but remaining below Class II and drinking-water limits by an order of magnitude; (3) release was time-limited: As stabilized within 12–24 h, Fe/Mn/Zn within 6 d, and Cu after a distinct secondary-release phase at 8–17 d, stabilizing by 24 d, whereas Ni rose gradually without reaching a plateau within the 8 d autumn campaign; (4) in the single pools tested, metal release was not monotonically related to module damage—the intact-module pool showed the highest Cu, Mn and Ni release—suggesting that corrosion of edge-mounted Cu components, rather than laminate breakage, controls long-term release; and (5) after scaling to the canal design discharge, PV-corridor-derived concentration increments are orders of magnitude below regulatory benchmarks even under the maximum observed interval release rate (~3.8×10^{-3} μg/L for Cu). For the measured dissolved analytes, the tested stagnant-immersion conditions and the initial 8–66 d exposure period examined here, we conclude that canal-top PV deployment on drinking-water transfer channels poses a low water-quality risk under normal operation, provided that corrosion-prone Cu components are properly specified, damaged modules and debris are removed promptly, and Cu, As and Ni are included in routine monitoring; constituents not measured in this study (e.g., microplastics, organic leachates, Ag, Al) warrant separate assessment before this conclusion can be generalized. The screening-level conclusion should be confirmed with replicated, statistically designed experiments.

Supplementary Materials: The following supporting information can be downloaded at: https://www.mdpi.com/article/10.3390/w18212728/s1, Table S1: Full time series of the parameters of Phase 1; Table S2: Full time series of the parameters of Phase 2.

Author Contributions: All authors contributed to the study conception and design. Conceptualization, A.Z.; methodology, Y.H. and L.M. (Lekang Ma); formal analysis, Y.H. and L.M. (Lekang Ma); investigation, L.M. (Lekang Ma) and L.M. (Leiming Meng); resources, L.M. (Leiming Meng) and X.S.; data curation, Y.H. and H.L.; writing—original draft preparation, Y.H. and Q.Y.; writing—review

and editing, Y.H.; visualization, Y.H. and Q.Y.; funding acquisition, A.Z. and Z.L. All authors have read and agreed to the published version of the manuscript.

Funding: This study was financially supported by the South-to-North Water Diversion Middle Route New Energy (Beijing) Co., Ltd. (Grant No. 202508251903).

Data Availability Statement: The original contributions presented in the study are included in the article/Supplementary Material; further inquiries can be directed to the corresponding author.

Acknowledgments: The authors sincerely thank LONGi Green Energy Technology Co., Ltd. and CHINT Group for providing the photovoltaic modules used in this study. We are also grateful to the laboratory staff for their technical assistance during the experiments. During the preparation of this manuscript, the authors used DeepSeek (V4) to debug Python scripts used for data processing and to draw Figure 3. The authors have reviewed and edited the output and take full responsibility for the content of this publication.

Conflicts of Interest: Authors An Zhou, Xiaodong Song, Leiming Meng, and Zhenghao Liu were employed by the company China South-to-North Water Diversion Renewables Investment Corporation Limited. The authors declare that this study received funding from China South-to-North Water Diversion Renewables Investment Corporation Limited. The funder was not involved in the study design, collection, analysis, interpretation of data, the writing of this article or the decision to submit it for publication.

Appendix A

Table A1. Experimental design of the two immersion campaigns.

Item	Phase 1 (Autumn)	Phase 2 (Spring)
Campaign period	11–19 September 2025 (0–192 h, 8 d)	Apr 17–Jun 22, 2026 (0–1584 h, 66 d)
Module models	LONGi P-type (PERC), N-type TOPCon, IBC	CHINT N-type TOPCon (4 damage levels), LONGi IBC (broken)
Treatments (pool no.)	1# P intact; 2# P broken; 3# TOPCon intact; 4# TOPCon broken; 5# IBC intact; 6# IBC broken	1# TOPCon severe (20% area); 2# moderate (10% area); 3# mild (5% area); 4# intact; 5# IBC broken
Blank	Two barrels (CK1, CK2) with tap water	Tap-water blank pool leaked during the campaign (no usable data); t = 0 sample of each pool used as background
Module size/weight	2382 × 1134 × 30 mm; 33.5 kg	2382 × 1134 × 30 mm; 31.65 kg (TOPCon)
Water	Tap water, static, outdoor, natural temperature, 2.6 m × 1.6 m × 0.35 m(±1.5 cm), 1497.6 L ± 260 L	Tap water, static, outdoor, natural temperature, 2.6 m × 1.6 m × 0.35 m(±1.5 cm), 1497.6 L ± 260 L
Pool	2.6 m × 1.6 m × 0.65 m, PVC-coated polyester-fabric pools (PVC sheet/polyester mesh/PVC sheet)	2.6 m × 1.6 m × 0.65 m, PVC-coated polyester-fabric pools (PVC sheet/polyester mesh/PVC sheet)
Sampling events	12	22
Analytes	Pb, Cd, As, Ni, phenol	Cu, Fe, Mn, Zn, Pb, Cd, Cr(VI), As, Hg, Ni
In situ parameters	T, EC, DO, turbidity	T, EC, DO, turbidity, TDS

Table A2. Analytical methods, detection limits and benchmark values.

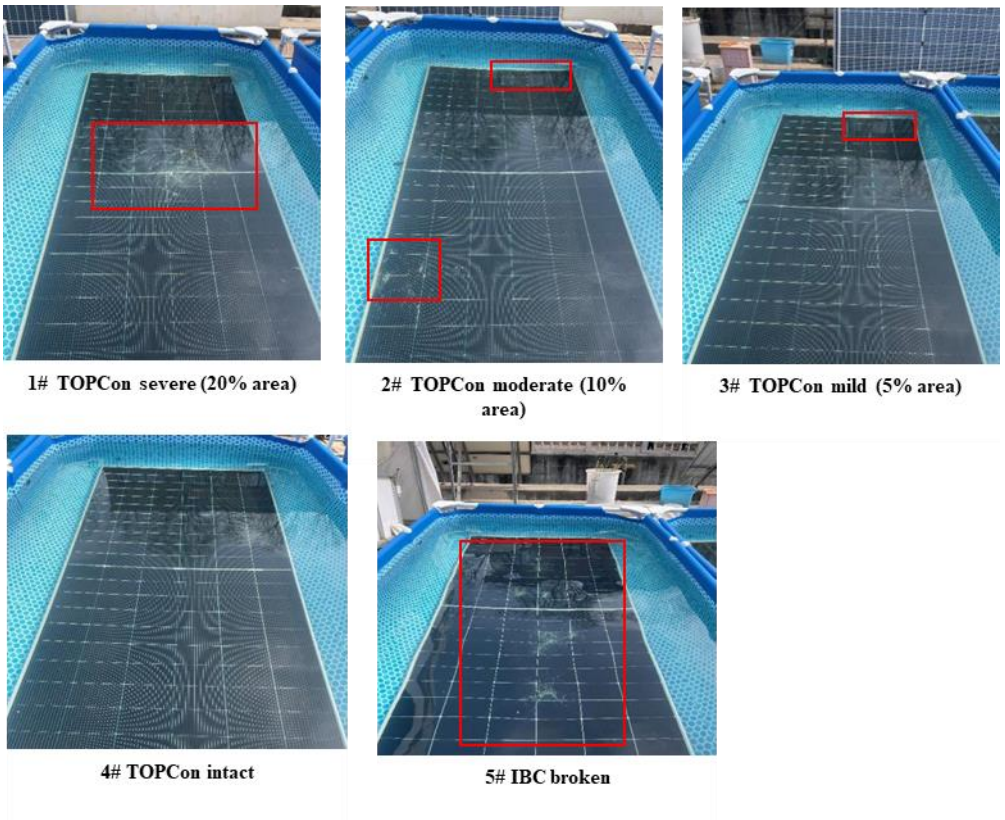
Analyte	Method (Standard)	LOD (μg/L)	GB 5749-2022 Limit (mg/L)	GB 3838-2002 Class I Limit (mg/L)	GB 3838-2002 Class II Limit (mg/L)
Cu	ICP-MS (HJ 700-2014)	0.08	1.0	0.01	1.0
Fe	ICP-MS (HJ 700-2014)	0.82	0.3	0.3 (source-water supplementary item)	0.3
Mn	ICP-MS (HJ 700-2014)	0.12	0.1	0.1 (source-water supplementary item)	0.1

Table A2. *Cont.*

Analyte	Method (Standard)	LOD (μg/L)	GB 5749-2022 Limit (mg/L)	GB 3838-2002 Class I Limit (mg/L)	GB 3838-2002 Class II Limit (mg/L)
Zn	ICP-MS (HJ 700-2014)	0.67	1.0	0.05	1.0
As	ICP-MS (HJ 700-2014)	0.12	0.01	0.05	0.05
Ni	ICP-MS (HJ 700-2014)	0.06	0.02 (expanded index)	/	/
Pb	ICP-MS (HJ 700-2014)	0.09	0.01	0.01	0.01
Cd	ICP-MS (HJ 700-2014)	0.05	0.005	0.001	0.005
Cr(VI)	GB/T 7467-87	4	0.05	0.01	0.05
Hg	Cold-vapor AAS (HJ 597-2011)	0.04	0.001	0.00005	0.00005
Phenol	continuous flow analysis spectrophotometry (SL/T 788-2019)	0.35	0.002	0.002	0.002



(**a**) Photo of Phase 1 (autumn)



(**b**) Photo of Phase 2 (spring)

Figure A1. Photographs of the Phase 1 (autumn) and Phase 2 (spring) experimental setups.

References

1. Pimentel Da Silva, G.D.; Branco, D.A.C. Is floating photovoltaic better than conventional photovoltaic? Assessing environmental impacts. *Impact Assess. Proj. Apprais.* **2018**, *36*, 390–400. [CrossRef]
2. Cagle, A.E.; Armstrong, A.; Exley, G.; Grodsky, S.M.; Macknick, J.; Sherwin, J.; Hernandez, R.R. The land sparing, water surface use efficiency, and water surface transformation of floating photovoltaic solar energy installations. *Sustainability* **2020**, *12*, 8154. [CrossRef]
3. Irandoostshahrestani, M.; Rousse, D.R. Status of photovoltaic water pumping systems in Iran: A comprehensive review. *Water Sci. Technol.* **2024**, *89*, 3270–3308. [CrossRef] [PubMed]
4. El Baradei, S.; Al Sadeq, M. Effect of solar canals on evaporation, water quality, and power production: An optimization study. *Water* **2020**, *12*, 2103. [CrossRef]
5. McKuin, B.; Zumkehr, A.; Ta, J.; Bales, R.; Viers, J.H.; Pathak, T.; Campbell, J.E. Energy and water co-benefits from covering canals with solar panels. *Nat. Sustain.* **2021**, *4*, 609–617. [CrossRef]
6. Panse-Aglave, G.; Hassan, Q. A review paper on energy harvesting in arid and semi-arid region via PV cell on irrigation canals. *Mater. Today Proc.* **2022**, *69*, 582–586. [CrossRef]
7. Kumar, M.; Kumar, A. Experimental validation of performance and degradation study of canal-top photovoltaic system. *Appl. Energy* **2019**, *243*, 102–118. [CrossRef]
8. Nong, X.; Shao, D.; Zhong, H.; Liang, J. Evaluation of water quality in the South-to-North Water Diversion Project of China using the water quality index (WQI) method. *Water Res.* **2020**, *178*, 115781. [CrossRef] [PubMed]
9. Dong, G.; Hu, Z.; Liu, X.; Fu, Y.; Zhang, W. Spatio-temporal variation of total nitrogen and ammonia nitrogen in the water source of the Middle Route of the South-To-North Water Diversion Project. *Water* **2020**, *12*, 2615. [CrossRef]
10. *GB 3838-2002*; Environmental Quality Standards for Surface Water; State Environmental Protection Administration. General Administration of Quality Supervision, Inspection and Quarantine of China: Beijing, China, 2002. (In Chinese)
11. Guo, Y.; Hua, J.; Zhu, Y.; Song, G.; Li, R.; Han, J.; Yang, L.; Zhou, B. Contents and risk assessment of heavy metals in surface water in the main canal of Middle Route of the South-to-North Water Diversion Project. *Acta Hydrobiol. Sin.* **2022**, *46*, 995–1006. (In Chinese with English abstract) [CrossRef]
12. Haas, J.; Khalighi, J.; de la Fuente, A.; Gerbersdorf, S.U.; Nowak, W.; Chen, P.-J. Floating photovoltaic plants: Ecological impacts versus hydropower operation flexibility. *Energy Convers. Manag.* **2020**, *206*, 112414. [CrossRef]
13. Exley, G.; Armstrong, A.; Page, T.; Jones, I.D. Floating photovoltaics could mitigate climate change impacts on water body temperature and stratification. *Sol. Energy* **2021**, *219*, 24–33. [CrossRef]
14. Nobre, R.; Boulétreau, S.; Colas, F.; Azemar, F.; Tudesque, L.; Parthuisot, N.; Favriou, P.; Cucherousset, J. Potential ecological impacts of floating photovoltaics on lake biodiversity and ecosystem functioning. *Renew. Sustain. Energy Rev.* **2023**, *188*, 113852. [CrossRef]
15. Benjamins, S.; Williamson, B.; Billing, S.-L.; Yuan, Z.; Collu, M.; Fox, C.; Hobbs, L.; Masden, E.A.; Cottier-Cook, E.J.; Wilson, B. Potential environmental impacts of floating solar photovoltaic systems. *Renew. Sustain. Energy Rev.* **2024**, *199*, 114463. [CrossRef]
16. Sandrini, G.; Wagenvoort, A.; van Asperen, R.; Hofs, B.; Mathijssen, D.; van der Wal, A. Illuminating the impact of a floating photovoltaic system on a shallow drinking water reservoir: The emergence of benthic cyanobacteria. *Water* **2025**, *17*, 1178. [CrossRef]
17. Pittaway, P.; Martínez-Alvarez, V.; Hancock, N.; Gallego-Elvira, B. Impact of artificial monolayer application on stored water quality at the air-water interface. *Water Sci. Technol.* **2015**, *72*, 1250–1256. [CrossRef] [PubMed]
18. Wang, X.; Zhao, Y.; Chu, Z.; Yu, X.; Fan, T.; Li, G.; Zhang, J.; Xu, X.; Zhen, Q.; Cheng, X.; et al. Influence of solar photovoltaic system on the concentration and environmental risks of heavy metals in subsidence pond water from coal mining area: A case study from Huainan subsidence pond. *Water* **2022**, *14*, 2257. [CrossRef]
19. Sinha, P.; Balas, R.; Krueger, L.; Wade, A. Fate and transport evaluation of potential leaching risks from cadmium telluride photovoltaics. *Environ. Toxicol. Chem.* **2012**, *31*, 1670–1675. [CrossRef] [PubMed]
20. Sinha, P.; Wade, A. Assessment of leaching tests for evaluating potential environmental impacts of PV module field breakage. *IEEE J. Photovolt.* **2015**, *5*, 1710–1714. [CrossRef]
21. Nain, P.; Kumar, A. Metal dissolution from end-of-life solar photovoltaics in real landfill leachate versus synthetic solutions: One-year study. *Waste Manag.* **2020**, *114*, 351–361. [CrossRef] [PubMed]
22. Nover, J.; Zapf-Gottwick, R.; Feifel, C.; Koch, M.; Werner, J.H. Leaching via weak spots in photovoltaic modules. *Energies* **2021**, *14*, 692. [CrossRef]
23. Tavolacci, B.C.; Nain, P.; Anctil, A. Aquatic toxicity of leachates from crystalline silicon photovoltaic components. *J. Environ. Manag.* **2025**, *382*, 125400. [CrossRef] [PubMed]
24. *GB 5749-2022*; Standards for Drinking Water Quality; State Administration for Market Regulation. Standardization Administration of China: Beijing, China, 2022. (In Chinese)

25. World Health Organization. *Guidelines for Drinking-Water Quality*, 4th ed.; Incorporating the First Addendum; World Health Organization: Geneva, Switzerland, 2017; ISBN 978-92-4-154995-0.
26. World Health Organization. *Guidelines for Drinking-Water Quality*, 4th ed.; Incorporating the First and Second Addenda; World Health Organization: Geneva, Switzerland, 2022; ISBN 978-92-4-004506-4.
27. European Union. Directive (EU) 2020/2184 of the European Parliament and of the Council of 16 December 2020 on the quality of water intended for human consumption (recast). *Off. J. Eur. Union* **2020**, *L435*, 1–62.
28. U.S. Environmental Protection Agency (USEPA). *Risk Assessment Guidance for Superfund, Volume I: Human Health Evaluation Manual (Part A), Interim Final*; EPA/540/1-89/002; USEPA: Washington, DC, USA, 1989.
29. Lin, L.; Zhang, Y.; Qian, X.; Wang, Y. Hydrochemical characteristics and human health risk assessment of surface water in the Danjiang River source basin of the Middle Route of China's South-to-North Water Transfer Project. *Water* **2023**, *15*, 2203. [CrossRef]
30. Zhang, C.; Duan, Q.; Yeh, P.J.-F.; Pan, Y.; Gong, H.; Gong, W.; Di, Z.; Lei, X.; Liao, W.; Huang, Z.; et al. The effectiveness of the South-to-North Water Diversion Middle Route Project on water delivery and groundwater recovery in North China Plain. *Water Resour. Res.* **2020**, *56*, e2019WR026759. [CrossRef]
31. Leuven, R.S.E.W.; Willems, F.H.G. Cumulative metal leaching from utilisation of secondary building materials in river engineering. *Water Sci. Technol.* **2004**, *49*, 197–203. [CrossRef]
32. Deng, R.; Chang, N.L.; Ouyang, Z.; Chong, C.M. A techno-economic review of silicon photovoltaic module recycling. *Renew. Sustain. Energy Rev.* **2019**, *109*, 532–550. [CrossRef]
33. Weckend, S.; Wade, A.; Heath, G. *End-of-Life Management: Solar Photovoltaic Panels*; Report T12-06:2016; International Renewable Energy Agency (IRENA) and International Energy Agency Photovoltaic Power Systems Programme (IEA-PVPS): Abu Dhabi, United Arab Emirates, 2016.
34. Xu, Y.; Li, J.; Tan, Q.; Peters, A.L.; Yang, C. Global status of recycling waste solar panels: A review. *Waste Manag.* **2018**, *75*, 450–458. [CrossRef] [PubMed]
35. de Oliveira, M.C.C.; Diniz Cardoso, A.S.A.; Viana, M.M.; Lins, V.D.F.C. The causes and effects of degradation of encapsulant ethylene vinyl acetate copolymer (EVA) in crystalline silicon photovoltaic modules: A review. *Renew. Sustain. Energy Rev.* **2018**, *81*, 2299–2317. [CrossRef]
36. d'Antonio, L.; Fabbricino, M.; Panico, A. Monitoring copper release in drinking water distribution systems. *Water Sci. Technol.* **2008**, *57*, 1111–1115. [CrossRef] [PubMed]
37. Galster, S.; Helmreich, B. Copper and zinc as roofing materials—A review on the occurrence and mitigation measures of runoff pollution. *Water* **2022**, *14*, 291. [CrossRef]
38. Segbefia, O.K.; Imenes, A.G.; Saetre, T.O. Moisture ingress in photovoltaic modules: A review. *Sol. Energy* **2021**, *224*, 889–906. [CrossRef]
39. Ramos-Ruiz, A.; Wilkening, J.V.; Field, J.A.; Sierra-Alvarez, R. Leaching of cadmium and tellurium from cadmium telluride (CdTe) thin-film solar panels under simulated landfill conditions. *J. Hazard. Mater.* **2017**, *336*, 57–64. [CrossRef] [PubMed]
40. Zhe, Y.; Pehkonen, S.O. Copper corrosion kinetics and mechanisms in the presence of chlorine and orthophosphate. *Water Sci. Technol.* **2004**, *49*, 73–81. [CrossRef]
41. Liu, W.; Guan, G.; Tian, X.; Cao, Z.; Chen, X. Exploiting a real-time self-correcting digital twin model for the middle route of the south-to-north water diversion project of China. *J. Water Resour. Plan. Manag.* **2023**, *149*, 04023023. [CrossRef]
42. Ali, S.Y.; Sunar, S.; Saha, P.; Mukherjee, P.; Saha, S.; Dutta, S. Drinking water quality assessment of river Ganga in West Bengal, India through integrated statistical and GIS techniques. *Water Sci. Technol.* **2021**, *84*, 2997–3017. [CrossRef] [PubMed]
43. Hurlbert, S.H. Pseudoreplication and the design of ecological field experiments. *Ecol. Monogr.* **1984**, *54*, 187–211. [CrossRef]
44. Larssen, T.; Carmichael, G.R. Acid rain and acidification in China: The importance of base cation deposition. *Environ. Pollut.* **2000**, *110*, 89–102. [CrossRef] [PubMed]

Disclaimer/Publisher's Note: The statements, opinions and data contained in all publications are solely those of the individual author(s) and contributor(s) and not of MDPI and/or the editor(s). MDPI and/or the editor(s) disclaim responsibility for any injury to people or property resulting from any ideas, methods, instructions or products referred to in the content.